Precipitation Induced Signatures in SAR Images

Andreas Danklmayer [#1], Madhukar Chandra [*2]

[#]*Microwaves and Radar Institute, German Aerospace Center(DLR)*
PO Box 1116, D - 82230 Wessling, Germany
[1]Andreas.Danklmayer@dlr.de

[*]*Dept. of Microwave Engineering and Photonics, Chemnitz University of Technology*
Raichenhainerstr. 70, D-09126 Chemnitz, Germany
[2]Madhu.Chandra@etit.tu-chemnitz.de

Abstract— **Active microwave SAR imaging of the Earth's surface is commonly considered to be of all weather capability. However, as the operating frequencies of SAR-systems are increasing, visible image distortions due to heavy precipitation in SAR-images are present. This holds especially for the case of convective rain events imaged at X–band frequencies and beyond. The German spaceborne satellite TerraSAR-X delivered several measurements, which facilitate to study precipitation effects in SAR-images. Based on this SAR-images and simultaneously acquired weather radar measurements, a quantitative estimation of precipitation effects in SAR-images is presented. In a further step, a first attempt is made to extrapolate the effects observed in X-band SAR images to images acquired at higher nominal frequency bands.**

I. INTRODUCTION

After the launch of TerraSAR-X in 2007 and during the commissioning phase, relevant images with raincell signatures were identified. The first image of TerraSAR-X provided in Fig. 1 gives an impression of how heavy rain may act on SAR images. The physical processes involved are

- reflection at the precipitation volume
- attenuation through the precipitation volume
- change of the surface due to the wetness and for water-surfaces due to the impinging rain drops or due to the influence by the wind

Today, a considerable body of literature exists on propagation effects in SAR imaging and how to make use of SAR data to deduce meteorological information. In the following we try to briefly review some of the more significant publications. The first contribution, which demonstrated the possiblity to apply SAR techniques to remote observations of meteorological targets was [1]. Others, such as [2], [3], [4], [5] followed. In [6] beside tropospheric effects also ionospheric effects are treated, however the ionosphere is considered irrelevant for frequency above 5 GHz, and thus we focus solely on the effects of precipitation, more specifically on rain attenuation and backscattering. An article which tries to evaluate rain-induced modification of X-band SAR performance is given in [7]. A remarkable contribution for the understanding of tropospheric effects in SAR images is due to [8] which is based on SIR-C/X data, which investigates signature of rain in SAR images over ocean surfaces, which is complicated as rain may cause changes of the water surface. Another contribution [9] is concerned with the limitations of SAR systems to measure rain. [10] considers the atmospheric loss of SAR systems in several different frequency bands in the presence of rain. In [11] tropospheric propagation effects in SAR imaging is addressed and several examples of TerraSAR-X datasets with visible artefacts are given. [12] is the most recent publication, which tries to invert SIR-C/X SAR data to derive precipitation over land.

This paper is organized as follows. In Section II we discuss the physical background of precipitation effects in SAR images. Moreover Section II-A aims at quantification of the observed effect of attenuation in two different nominal frequencies, the X-band (9.65 GHz) and at Ka-band frequencies more specifically at 35 GHz. In Section II-B we calculate the rainfall rate, which is necessary to produce visible artefacts in Ka-band SAR images for the modelled scenario. A last section (II-C) is devoted to briefly address the issue of which regions on Earth are most likely affected in dependence of the annual rainfall. Finally in the conlusion provided in Section III, we briefly summarize the obtained results and shall give an outlook on open issues to be investigated in the next future.

II. ANALYSIS OF DATASETS AND PHYSICAL INTERPRETATION OF ARTEFACTS IN SAR IMAGES DUE TO PRECIPITATION

A physical interpretation of how rain cells affect SAR images is given in Fig. 2. The sketch shows an imaging scenario, where the transmitted waves interact with a precipitation cell. The red rays correspond to the signals transmitted through the clouds, the black rays to the reflected ones. It can be observed, that at area 'A' which corresponds to time instant τ_A in the amplitude/time diagram, is due to strong backscattering from large hydrometeors. Time instant τ_B, which corresponds to the region 'B' proves that signals have been heavily attenuated. By comparing the encircled area in Fig. 1 and the amplitude/time diagram in Fig. 2, the veil in Fig. 1 corresponds to area 'A' (τ_A) and the shadow like black areas close to these veil in Fig. 1 corresponds to the region 'B' (τ_B) in Fig. 2.

In additon to the effects discussed above, the well known layover effect may occur due to the precipitation volume, since the echo from the rain (precipitation) volume within the
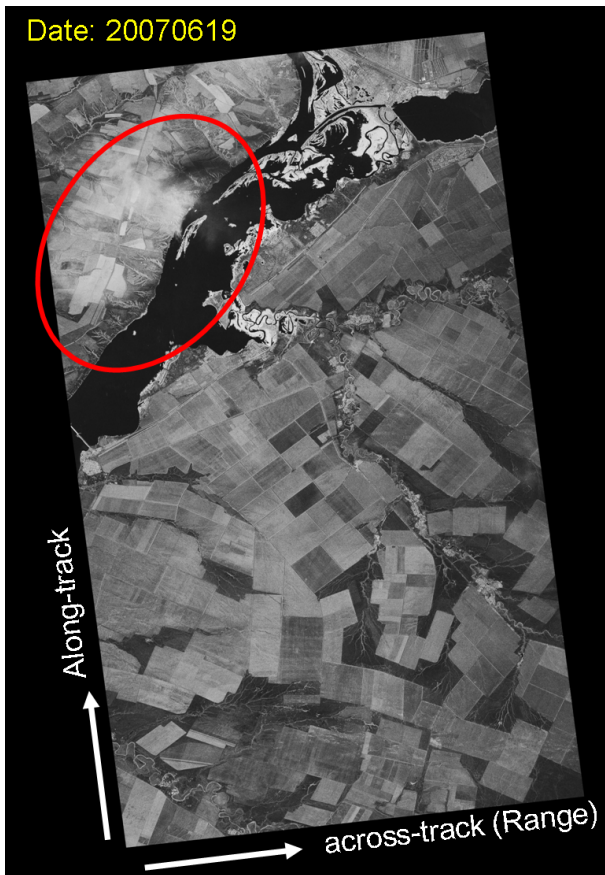
Fig. 1. An example of rain-cell-affected SAR signatures recorded with TerraSAR–X. The white shading is due to direct reflections from the rain region (shown as volume 'A' in Fig. 2). Whereas the darkly shaded areas are due to rain attenuated (blocked) signals from the ground; this effect is shown as region 'B' in Fig. 2. The parameters of acquisition are given in Table I.

TABLE I

THE MAIN ACQUISITION PARAMETERS OF THE FIRST IMAGE ACQUIRED BY TERRASAR–X OBTAINED 4.5 DAYS AFTER LAUNCH.

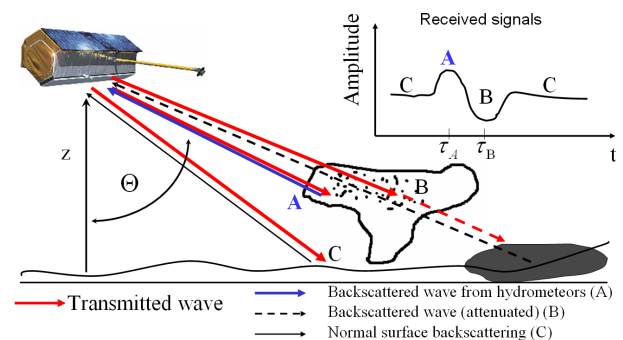| Parameter	Values
Frequency band	X–band / 9.65 GHz
Image dimensions:	Azimuth $\sim$ 60 km
	Range $\sim$ 30 km
Location	50 km to the west of
	Volgograd (Russia)
Scene center	Lat: 48.4504
	Lon: 43.5542
Imaging Mode	Strip map / HH Polarization

Fig. 2. A physical interpretation of rain cell signatures in SAR-images, as indicated and introduced previously in Fig. 1.

resolution cell is superimposed to the echo from the ground, as shown digaramatically in Fig.3.

In Fig. 6, a comparison between X-band SAR measurements with measurements from a ground based weather radar is given. A good overall agreement can be observed. For X-band frequencies heavy precipitation with reflectivities up to 50 dBZ causes pronounced visible artefacts in SAR images.

A. Attenuation through rain

One of the major problems affecting microwave and mil-limetre wave bands for terrestrial and space-borne radars is the attenuation through rain [13], [7]. Rain is the most important cause, not only due to the strong attenuation effect but also due to the fact that rain occurs most frequently. A convenient way to describe the rain intensity is the so called rainfall-rate or rain-rate given in millimetres per hour. This quantity refers to a certain flux of rain towards the surface of the Earth and may be measured e.g. by gauges or weather radars. A rain rate of 4 mm/hr is a typical value for the specification of moderate rain [13]. Typical values for the specific attenuation (attenuation for 1 km propagation path) of different frequency bands according to a given rain-rate are provided in [14]. A
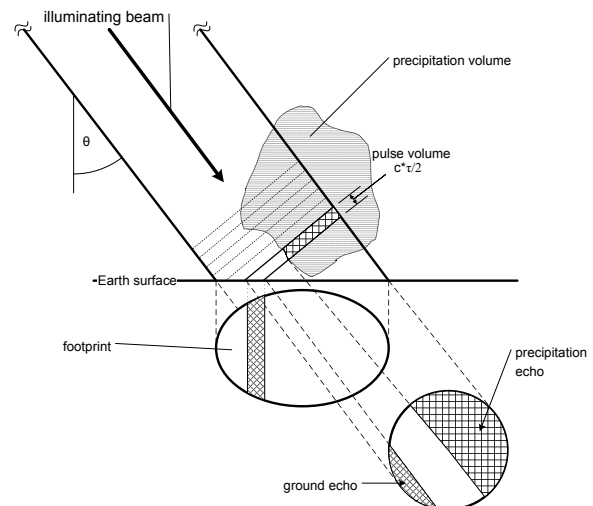

Fig. 3. A depiction of a SAR imaging scenario which illustrates the layover effect. As digarammatically shown the ground responses are superimposed by the backscattering from corresponding range cells of the precipitation volume (adopted from [9]).
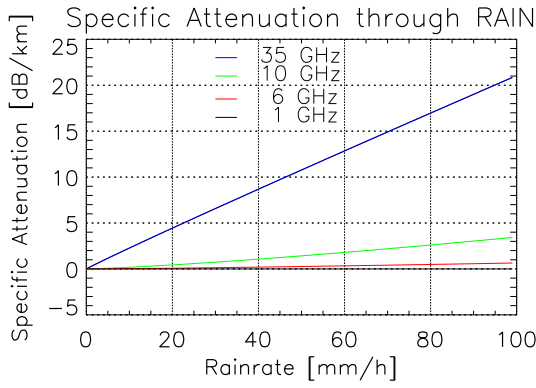
Fig. 4. A plot of the specific attenuation given in units of dB/km versus the rain rate in units of mm/hr for four different frequencies (1, 6, 10 and 35 GHz) after the ITU Model Recommendation 838 (1994).

widely acceped empirical relation of the form

$$\gamma(x,t) = a \cdot R^b \qquad (1)$$

between specific attenuation $\gamma(x,t)$ and rain rate R is used to calculate the specific attenuation for a given rain rate [13], [15], [16]. The parameters a and b are dependent on the radio frequency, the raindrop size distribution, the polarization and other factors [15].

After [13], the total attenuation for a given instant of time can be obtained by adding up the specific attenuation along the path of propagation using the following expression

$$A(t) = \int_0^{2h} \gamma(x,t)dx \qquad (2)$$

where

$A(t)$	...total attenuation for given time instant t
t	...time
h	...path length
$\gamma(x,t)$	...specific attenuation
x	...position along the path of propagation

The specific attenuation along the slant path of propagation has to be known. However, detailed knowledge of the medium through which the signal propagates is rather limited and the temporal and spatial variation of the medium require assumptions and some modelling [10]. In the case of precipitation we may have some idea about the thermodynamic phase (ice, water, melting band) but no precise information. Using the calculated values for the specific attenuation in X-band provided in diagram Fig. 4 for a 5 km long path through a heavy tropical convective rain (70 mm/hr and more) suggests a 20 – 30 dB attenuation, which was confirmed by comparing the backscattering coefficient of affected and non–affected region from data takes acquired by TerraSAR-X over Brazilien rain forest.
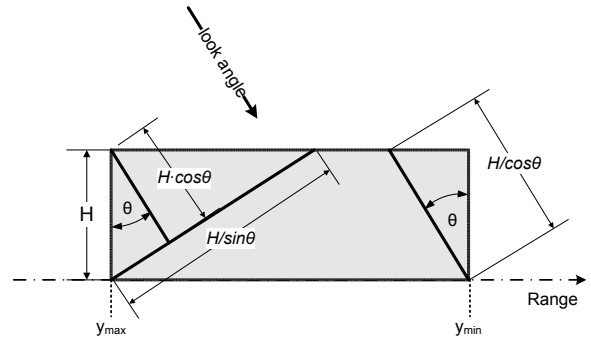

Fig. 5. The structure of an idealised rain cell used for the calculation in Section II-B.

B. Modelling of the Attenuation under Rain Conditions for Ka-band

For the calculations of the rain rate to cause visible attenuation in Ka-band SAR images, a simple model shown in Fig. 5 [8], is used. A reasonable height of 4 km is assumed, as well as a homogenous rain rate for the modelled cell. The incidence angle of the propagating signals was chosen 30°. With the help of (1) and by using the regression coefficients in Table II, the specific attenuation was calculated. These values are given in Table III. Finally, the values for the two-way path attenuation for different rain rates (5, 50 and 100 mm/hr) can be found in Table IV.

As a total two-way attenuation of 25 dB becomes visible in SAR images in X-band it is of interest which rain rate is necessary to cause such an attenuation for Ka-band (35 GHz) frequencies. To this end, the following equation is applied

$$\gamma(t) = \frac{A(t)}{2 \cdot \frac{H}{\cos(\theta)}} \qquad [dB/km] \qquad (3)$$

where the rain rate is found using (1) with the according parameters a and b for Ka-band.

$$R = \sqrt[b]{\frac{\gamma(t)}{a}} \qquad (4)$$

First calculations using the parameters of the idealised rain cell of 4 km and using 25 dB of total two-way attenuation, assuming the Marshall Pallmer Parameters for Ka-band attenuation deliver a rain rate close to 10 mm/hr. This simple example demonstrates that such rain rates are fully capable to distort Ka-band SAR measurements to a visible extent. In addition to the aforementioned simple assumptions of a homogenous rain cell with constant precipitation may be somehow optimistic, since a melting layer precipitation may severly increase the total path attenuation.

C. Probability of Rain Events

Some basic meteorological facts concerning rain, clouds and precipitation are briefly summarized in the following [9]:

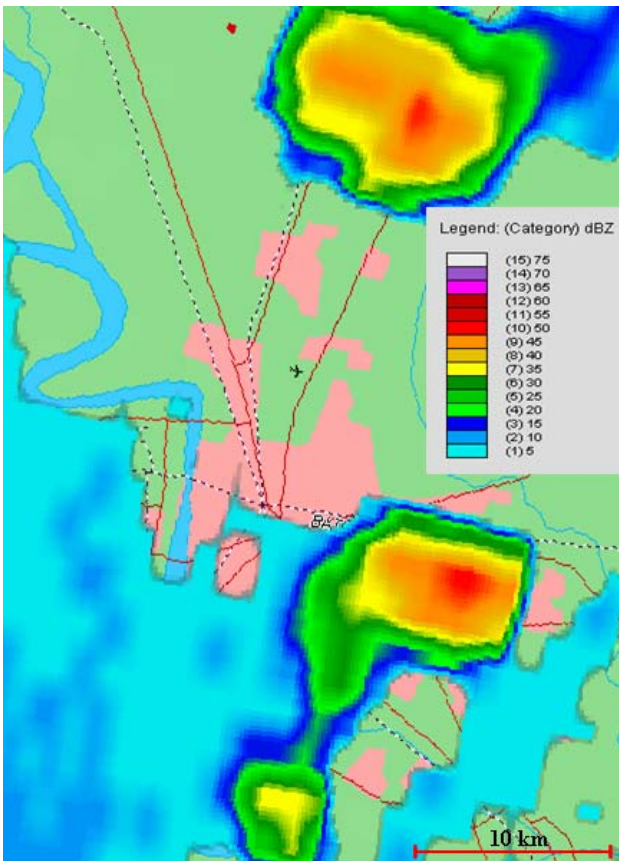- On average, 50 % of the Earth's surface is coverered by clouds

Fig. 6.   A test case showing a comparison of X-band TerraSAR-X data and weather radar data (Nexrad, NOAA) acquired nearly simultaneously (within the same minute) over a scene close to New Orleans, US. A good agreement between the rain-cell signatures in the SAR image (right hand side) and the weather radar image (left hand side) can be observed. The effects are most pronounced for reflectivieties of up to 50 dBZ.

TABLE II

REGRESSION COEFFICIENTS USED FOR THE CALCULATION OF THE SPECIFIC ATTENUATION CF. (1)

| Frequency | DSD | | | |
| | Marshall Pallmer | | Joss Thunderstorm | |
	a	b	a	b
X-Band (10 GHz)	0.0136	1.15	0.0169	1.076
Ka-Band (35 GHz)	0.268	1.007	0.372	0.783

TABLE III

SPECIFIC ATTENUATION $[dB/km]$

| Rainrate [mm/hr] | Specific Attenuation | |
	10 GHz	35 GHz
5	0.08	1.31
50	1.22	7.95
100	2.4	13.69

TABLE IV

MAXIMUM ATTENUATION FOR MODELLED RAIN CELL $[dB]$

| Rainrate [mm/hr] | Specific Attenuation | |
	10 GHz	35 GHz
5	0.739	12.1
50	11.26	73.43
100	22.17	126.46

- the rain to cloud ratio is seldom larger than 10 %
- the upper bound is 5 % on Earth's surface receiving rain at a given time
- rain events are dominated by light rain events, however higher rain rates account for most of the total liquid water reaching the surface
- even for the areas with the highest rain rate, the percentage time in a year (annual probability) that exceeds 50mm/hr is 0.1 % (526 min)
- 150 mm/hr is exceeded less than 0.01 % (53 min)

A graphical depiction showing the total amount of rain in mm/year is given in Fig. 7, where regions receiving larger amounts of rain fall can be easily identified. Images from such regions are most likely affected by attenuation effects due to heavy precipitation.

III. CONCLUSIONS

Considerable physical insight into precipitation induced signature in SAR images is provided based on data examples
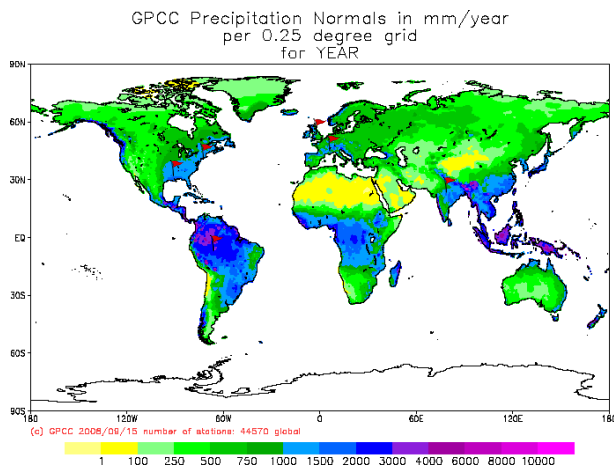
GPCC Precipitation Normals in mm/year
per 0.25 degree grid
for YEAR

Fig. 7. A depiction of the global distribution of the annual amount of rain fall in mm/y. The flags in red indicate the locations of selcted relevant datasets of TerraSAR-X, which were used for the investigations in this contribution.

acquired with the space-borne SAR sensor TerraSAR–X. As theoretically expected, the comparison between simultanously measured weather radar and SAR data demonstrated clearly that heavy precipitation (> 50 dBZ) cause visible artefacts in SAR images. For SAR systems operating at higher frequency bands, i.e. for a Ka-band system (nominal frequency of $35\,$GHz) an estimation of the critical rain rate that may cause visible artefacts in SAR images is given. TerraSAR-X offers new and intriguing possibilities to study propagation effects in SAR images and furthermore to retrieve meteorological information by using SAR measurements.

REFERENCES

[1] D. Atlas, C. Elachi, and J. W. E. Brown, "Precipitation mapping with airborne synthetic aperture imaging radar," *J. of Geophys. Res.*, vol. 82, pp. 3445 –3451, 1977.
[2] J. Metcalf and W. Holmes, "Meteorological applications of synthetic aperture radar," Georgia Institute of Technology, Tech. Rep., 1979, prepared for Laboratory for Atmospheric Sciences of NASA.
[3] D. Atlas and R. K. Moore, "The Measurements of Precipitation with Synthetic Aperture Radar," *Journal of Atmospheric and Oceanic Technology*, vol. 4, pp. 368–376, 1987.
[4] A. Pichugin, Y. G. Spiridonov, and A. B. Fetisov, "Spatial Structure of Liquid Precipitation Fields in Space Radar Imagery taken at two Orthogonal Polarizations," *Issled. Zemli iz Kosmosa*, vol. 7, no. 4, pp. 70–77, 1987.
[5] A. Pichugin and Y. Spiridonov, "Spatial distribution of rainfall intensity recovery from space radar images," *Sov. J. Remote Sensing*, vol. 8, pp. 917–932, 1991.
[6] S. Quegan and J. Lamont, "Ionospheric and tropospheric effects on synthetic aperture radar performance," *International Journal of Remote Sensing*, vol. 7, no. 4, pp. 525–539, 1986.
[7] P. Ferrazzoli and G. Schiavon, "Rain-induced modification of SAR performance," *Adv. Space Res.*, vol. 7, no. 11, pp. 269–272, 1987.
[8] C. Melsheimer, *Signaturen von Regen in Radaraufnahmen des Meeres*. Aachen: Shaker Verlag, 1998.
[9] A. Ahamad, "Limitation on the use of a space-borne SAR for rain measurements," Radar Systems and Remote Sensing Laboratory, Department of Electrical Engineering and Computer Science, University of Kansas, University of Kansas, Tech. Rep. RSL Technical Report 8370-4, 1994.
[10] A. W. Doerry, "Atmospheric loss considerations for synthetic aperture radar design and operation," in *Proceedings of SPIE*, 2004.
[11] A. Danklmayer, "Propagation effects and polarimetric methods in synthetic aperture radar (SAR) imaging," Ph.D. dissertation, Chemnitz University of Technology, DLR-Report FB-2008-14, Technical University of Chemnitz, 2008.
[12] F. S. Marzano and J. A. Weinman, "Inversion of space-borne X-band synthetic aperture radar measurements for precipitation remote sensing over land," *IEEE Transactions on Geoscience and Remote Sensing*, vol. 46, no. 11, pp. 3472–3487, Nov. 2008.
[13] R. K. Crane, *Electromagnetic wave propagation through rain*. John Wiley and Sons, 1996.
[14] ITU, *Recommendation 838, propagation in non-ionized media*, 1994.
[15] R. L. Olsen, D. V. Rogers, and D. B. Hodge, "The $a \cdot R^b$ relation in calculation of rain attenuation," *IEEE Transactions on Antennas and Propagation*, vol. 26, no. 2, pp. 318–329, 1978.
[16] V. N. Bringi and V. Chandrasekar, *Polarimetric Doppler weather radar, principles and applications*. New York: Cambridge University Press, 2001.